J. Fluid Mech. (1969), *vol.* 37, *part* 1, *pp.* 129–147
Printed in Great Britain

Turbulent boundary-layer flow on a rotating disk

By T-S. CHAM AND M. R. HEAD
Cambridge University Engineering Department

(Received 1 November 1968)

Calculations have been made of the development of the turbulent boundary layer on a disk rotating in free air, using circumferential and radial momentum-integral equations and an auxiliary equation of entrainment. In the calculations, circumferential velocity profiles are represented by Thompson's (1965) two-parameter family, while radial profiles are given by Mager's (1952) quadratic expression. The circumferential component of skin friction follows from the use of Thompson's profile family for the circumferential velocity. The entrainment, in dimensionless form, is assumed to be determined uniquely by the circumferential velocity profile in the same way as was proposed by Head (1958) for a two-dimensional turbulent boundary layer.

Detailed measurements have been made of the development of the turbulent boundary layer on the rotating disk, and the calculations are found to be in excellent agreement with the results when a suitable adjustment is made to Head's two-dimensional entrainment curve.

1. Introduction

One of the simplest types of three-dimensional boundary-layer flow† is that induced by a disk rotating in its own plane in a fluid at rest at infinity. The fluid adjacent to the disk rotates with it and so is subjected to centrifugal forces which cause it to flow outwards, the disk thus acting like an inefficient centrifugal impeller.

Several different régimes of flow exist, distinguished by values of the Reynolds number ($\Omega r^2/\nu$) based on radius and rotational velocity. For sufficiently low Reynolds numbers the flow is laminar and the equations for this case have been formulated by von Kármán (1921) and solved by Cochran (1934). Similar transformations to those used for axisymmetric stagnation point flow reduce the partial differential equations to a pair of ordinary differential equations, and the noteworthy features of the solution for stagnation point flow, invariance with radius of boundary-layer thickness and velocity distribution through the layer, reappear in the solution for the rotating disk.

At a Reynolds number of approximately $1{\cdot}85 \times 10^5$ the laminar flow becomes unstable and breaks down into a series of discrete spiral vortices. This second equilibrium state becomes unstable in turn, breaking down to general turbu-

† The term 'three-dimensional' is used here in the sense which is customary for boundary layers (see, for example, Rosenhead 1963) although it is, of course, recognized that, in the present case, there is no variation in the azimuthal direction.

lence, the transition process being complete at a Reynolds number of $2{\cdot}85 \times 10^5$. These experimental results were reported by Gregory, Stuart & Walker (1955) and are largely confirmed in the present work. Possibly because the instability of the basic laminar flow and (presumably) that of the equilibrium spiral flow that succeeds it is dynamic in origin, rather than viscous, the transition process appears to be very much more regular and reproducible than it is, for example, in the case of a flat plate in a uniform stream, and it is to be expected that the turbulent boundary-layer characteristics will be, to a close approximation, uniquely determined by the Reynolds number.

The object of the present investigation has been to obtain reasonably complete and detailed measurements of the turbulent boundary-layer development, which can be used as a check of proposed methods of calculating the development of three-dimensional turbulent boundary layers. Both from the point of view of experiment and analysis, it represents a comparatively simple problem and one that, in a particular sense, is complementary to the attachment line flow described by Cumpsty & Head (1967); that flow is characterized by divergence of the external streamlines and zero cross-flow, whereas in the present case flow divergence is absent but cross-flow is an essential characteristic.

The method used by Cumpsty & Head (1967) to calculate turbulent boundary-layer development on an infinite swept wing has been applied to the rotating disk flow and has been found to give excellent agreement with the measurements, but only if the entrainment is reduced to approximately two-thirds of the flat plate value. Thus the present results cannot be said to confirm the overall validity of the method.

The only previous measurements of the turbulent boundary layer on a rotating disk known to the authors were reported by Gregory *et al.* (1955) and Stain (1961), and these were not comprehensive. Earlier experiments by Schmidt (1921), Kempf (1922) and Theodorsen & Regier (1944) were confined to the measurement of torque. Calculations for the turbulent boundary layer, again mainly directed at establishing the skin-friction drag and resisting torque, have been performed by von Kármán (1921), Goldstein (1935), Dorfman (1963) and Banks & Gadd (1962). Comparisons of their theories with the present measurements show that their overall predictions are far from satisfactory, especially at the lower Reynolds numbers.

2. Boundary-layer equations

The Navier–Stokes equation in a uniformly rotating co-ordinate system may be written as

$$\mathbf{a} + 2\boldsymbol{\omega} \times \mathbf{v} + \boldsymbol{\omega} \times (\boldsymbol{\omega} \times \mathbf{r}) = -(1/\rho)\nabla p + \nu \nabla^2 \mathbf{v}, \tag{1}$$

where $\mathbf{a}$ is the acceleration vector, $\boldsymbol{\omega}$ is the rotation vector of the co-ordinate system, $\mathbf{v}$ is the velocity vector, $\mathbf{r}$ is the position vector, ρ is the density of the fluid, p is the pressure, and ν is the kinematic viscosity.

The continuity equation for an incompressible flow is

$$\nabla . \mathbf{v} = 0. \tag{2}$$

A cylindrical co-ordinate system is chosen with the z-axis coinciding with the axis of rotation. Using a notation where ξ represents the distance measured along a circle of radius r, η is the distance measured in the radial direction and ζ is the distance normal to the disk, it is easily seen that

$$d\xi = r\,d\theta, \quad d\eta = dr, \quad d\zeta = dz.$$

By expanding equation (1), introducing the boundary-layer approximations and taking mean values, the equations for a turbulent boundary layer, referred to the rotating co-ordinate system, are obtained as

$$u\frac{\partial u}{\partial \xi} + v\frac{\partial u}{\partial \eta} + w\frac{\partial u}{\partial \zeta} + \frac{uv}{r} + 2\Omega v = -\frac{1}{\rho}\frac{\partial p}{\partial \xi} + \frac{1}{\rho}\frac{\partial \tau_1}{\partial \zeta}, \tag{3}$$

$$u\frac{\partial v}{\partial \xi} + v\frac{\partial v}{\partial \eta} + w\frac{\partial v}{\partial \zeta} - \frac{u^2}{r} - 2\Omega u - \Omega^2 r = -\frac{1}{\rho}\frac{\partial p}{\partial \eta} + \frac{1}{\rho}\frac{\partial \tau_2}{\partial \zeta}, \tag{4}$$

$$0 = -\frac{1}{\rho}\frac{\partial p}{\partial \zeta}, \tag{5}$$

where u, v and w are components of the mean velocity in the circumferential, radial and axial directions respectively, Ω is the rate of rotation, and τ_1, τ_2 are the shear-stress components (including Reynolds stresses) in the circumferential and radial directions.

The continuity equation becomes

$$\frac{\partial u}{\partial \xi} + \frac{\partial v}{\partial \eta} + \frac{\partial w}{\partial \zeta} + \frac{v}{r} = 0. \tag{6}$$

By (5), and the fact that the pressure outside the boundary layer is uniform, terms involving differentials of p can be ignored.

3. Momentum-integral equations

By integrating equations (3) and (4) with respect to ζ from 0 to d, where $d \geqslant \delta$, and noting that $U = -\Omega r$ in a right-handed orthogonal co-ordinate system, where U is the velocity outside the boundary layer, the following integral equations are obtained:

$$\frac{\partial \theta_{12}}{\partial \eta} + \frac{4\theta_{12}}{r} = \frac{\tau_{01}}{\rho U^2}, \tag{7}$$

and

$$\frac{\partial \theta_{22}}{\partial \eta} + (3\theta_{22} + \theta_{11} - \delta_1^*)/r = -\frac{\tau_{02}}{\rho U^2}, \tag{8}$$

where the signs of the θ_{12} terms have been changed to allow for positive U and u, since the terms are actually negative with respect to the rotating right-handed co-ordinate system. The various boundary-layer thicknesses are defined by

$$\delta_1^* = \frac{1}{U}\int_0^\delta (U-u)\,d\zeta, \qquad \delta_2^* = \frac{1}{U}\int_0^\delta v\,d\zeta.$$

$$\theta_{11} = \frac{1}{U^2}\int_0^\delta (U-u)u\,d\zeta, \quad \theta_{12} = \frac{1}{U^2}\int_0^\delta (U-u)v\,d\zeta,$$

$$\theta_{21} = \frac{1}{U^2}\int_0^\delta uv\,d\zeta, \qquad \theta_{22} = \frac{1}{U^2}\int_0^\delta v^2\,d\zeta.$$

τ_{01} and τ_{02} are the wall-shear-stress components in the circumferential and radial directions respectively.

Equations (7) and (8) can be shown to be a particular case of the general equations derived by Mager (1952) for a rotating co-ordinate system.

An entrainment equation can be derived from continuity considerations. Take a boundary normal to the disk at radius r. The volume flow, Q, rate across the boundary is given by

$$Q = \int_0^\delta 2\pi r v \, d\zeta = 2\pi r U \delta_2^*,$$

and, noting that U is proportional to r, the rate of change of the flow is obtained as

$$\frac{dQ}{dr} = 2\pi U \left(r \frac{\partial \delta_2^*}{\partial r} + 2\delta_2^* \right).$$

The additional fluid is supplied from outside the boundary layer, and dQ is the entrainment rate across the band width dr of the boundary layer at radius r. An entrainment coefficient, C_E, can be defined for this case by

$$C_E = \frac{1}{2\pi U r} \frac{dQ}{dr} = \frac{\partial \delta_2^*}{\partial r} + 2\frac{\delta_2^*}{r}. \tag{9}$$

Equation (9) will serve as an auxiliary equation if C_E can be empirically related to other boundary-layer parameters.

4. Additional assumptions and method of solution

The equations to be satisfied are the streamwise and cross-flow momentum-integral equations (7) and (8) and the equation of entrainment (9). To obtain a solution to these equations, the following assumptions are made.

(i) It is assumed that the streamwise velocity profiles correspond to Thompson's (1965) two-dimensional family, where

$$\frac{u}{U} = \frac{u}{U}(H, R_\theta, y/\theta),$$

the two-dimensional momentum thickness θ being replaced by the streamwise momentum thickness θ_{11} in the momentum thickness Reynolds number $R_\theta \, (\equiv U\theta/\nu)$. The velocity profile shape factor H is given by δ_1^*/θ_{11}.

(ii) The cross-flow velocity profile is assumed to correspond to the cross-flow model proposed by Mager (1952), i.e.

$$\frac{v}{U} = \frac{u}{U}(1 - \zeta/\delta)^2 \tan\beta,$$

where β is the angle the limiting surface streamline makes with the main flow direction and is related to the wall shear stress components by

$$\tan\beta = \lim_{\zeta \to 0} \left(\frac{v}{u} \right) = \frac{\tau_{02}}{\tau_{01}}.$$

For the present calculation, δ is defined as the value of ζ where $u/U = 0{\cdot}995$.

(iii) The streamwise component of skin friction, τ_{01}, is calculated using Thompson's skin-friction relation $C_f = C_f(R_\theta, H)$, the two-dimensional momentum thickness θ being replaced by the streamwise momentum thickness θ_{11}. Thompson's skin friction relationship is at least as reliable as alternative proposals and is, moreover, consistent with the choice of streamwise velocity profiles.

(iv) C_E is identified with the F function of Head (1958) for two-dimensional turbulent boundary layers and is an empirical function. The present extension to three dimensions assumes that the streamwise (i.e. circumferential) component behaves as a two-dimensional flow with regard to entrainment and that

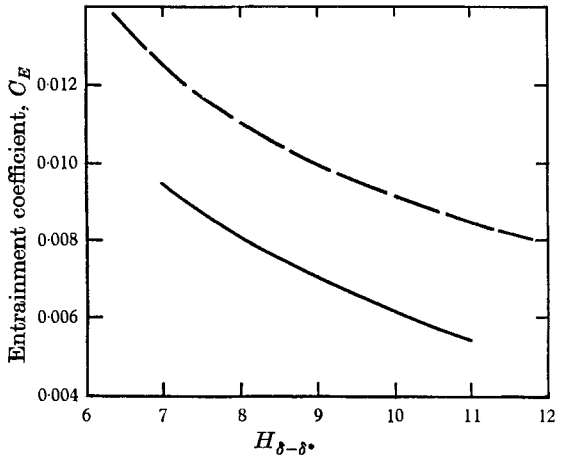

FIGURE 1. Entrainment functions. ———, Head (1958); ——, present calculation.

the cross-flow component makes a negligible contribution. Following Head's assumption for two-dimensional flow, we therefore write

$$C_E = C_E(H_{\delta-\delta_1^*}).$$

Values of $H_{\delta-\delta_1^*}$, which is given by $(\delta-\delta_1^*)/\theta_{11}$, are related to corresponding values of H and $R_{\theta 11}$ by Thompson's profile family, in which velocity profiles are specified as functions of H and R_θ.

It is found that for best overall agreement between experiment and theory, appreciably lower entrainment than that proposed by Head for a two-dimensional flow must be used, as indicated in figure 1. This lower entrainment rate is confirmed later by direct measurements (see § 6).

The technique of solution used is essentially a simultaneous solution of equations (7), (8) and (9), and only one initial condition is required. The aim is to solve for H, θ_{11} and $\tan\beta$ for the full extent of the turbulent boundary layer on the disk, with a starting value of θ_{11} at a certain radius.

Since the cross-flow is specified by the streamwise flow and the surface yaw angle, all the cross-flow thicknesses in equations (7), (8) and (9) are more conveniently expressed as functions of $\tan\beta$ and θ_{11}. For example, $\delta_2^* = A\theta_{11}\tan\beta$, where A is a coefficient dependent on H and $R_{\theta 11}$.

At the starting point, as θ_{11} is known, τ_{01} and $\tan\beta$ are solved simultaneously from equations (7) and (8). The derivatives in the radial (i.e. cross-flow) direction in both the equations are eliminated by equation (9). It must be noted that only $\tan\beta$ is obtained explicitly, H being deduced from the skin friction relation $C_{f1} = C_{f1}(H, R_{\theta 11})$, where $C_{f1} = \tau_{01}/\frac{1}{2}\rho U^2$. When the first step is completed, by equation (9), the radial gradient of streamwise momentum thickness θ_{11} can be determined. This leads to a new θ_{11} value at a new radius, and the whole calculation is repeated. In this manner, the calculation proceeds by finite steps from streamline to streamline, the steps being sufficiently small to ensure an accurate solution.

The computer calculation, which was carried out on the Cambridge Titan computer may be outlined as follows.

As a first approximation, the gradient of θ_{11} in the radial direction was assumed to be very much greater than the corresponding gradients of H and $\tan\beta$ and terms involving derivatives of these quantities were therefore neglected. H, $R_{\theta 11}$ and $\tan\beta$ were thus obtained for the range of radius of interest. From this initial calculation, the derivatives which had been neglected were estimated and included in the calculation for the next approximation. This procedure was repeated until two successive solutions were effectively identical. The starting value of θ_{11} for the turbulent boundary layer was taken from measurements by Gregory *et al.* (1955) and its accuracy is confirmed by the present experimental results.

The solution showed that H, $\tan\beta$ and C_{f1} decrease slowly with respect to radius whereas θ_{11} increases rapidly. Thus, the initial solution, where the derivatives of H and $\tan\beta$ were neglected in comparison with those of θ_{11}, differed from the final solution by not more than 5 %.

5. Apparatus and experimental techniques

The basic experimental apparatus consisted of a steel disk 3 ft. in diameter and $\frac{1}{2}$ in. thick which was flat to $\pm 0{\cdot}0015$ in. It was supported on a thrust bearing, mounted on a rigid steel frame. The vertical spindle was aligned by two ball bearings 2 ft. 3 in. apart and was driven by a 2 hp a.c. motor. By means of a Variac control, the rotational speed could be set for any value up to 1900 rev/min. The speed was continuously checked by a stroboscope. Very little vibration was observed except near a resonant frequency at approximately 1300 rev/min.

Boundary-layer measurements were made using stationary probes which could be traversed both radially and vertically as well as rotated in yaw. Vertical movement was indicated on a dial guage measuring in thousandths of an inch and the angle in yaw could be read on a Vernier scale to 5 minutes of arc, which was considerably greater than the accuracy with which flow angles could actually be determined.

Two different probes were used. The first consisted of three flattened Pitots soldered side by side so as to form a Conrad tube with an overall width of approximately 0·10 in. The flattened tips had an overall depth of 0·010 in. with openings 0·005 in. deep. The two outer tubes were connected across a sensitive manometer,

and yaw was indicated by the position for null reading. The centre tube was connected to an alcohol manometer, the low pressure side of which was left open to atmosphere. It was assumed that the static pressure throughout was equal to room pressure. Measurements of flow direction made using this probe as a yaw-

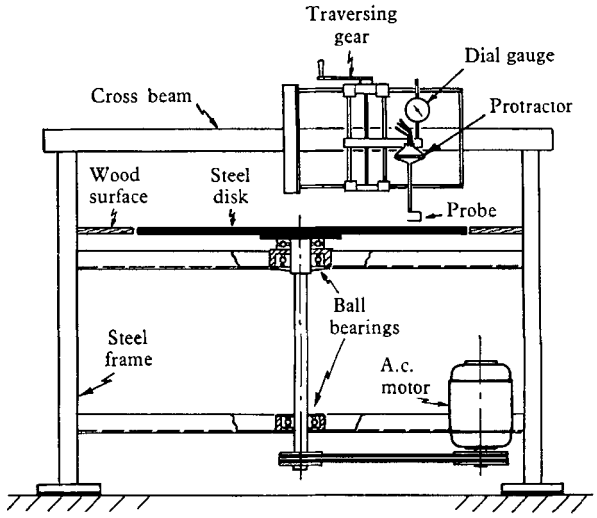

FIGURE 2. Schematic diagram of the experimental arrangement.

meter were never entirely satisfactory and, later, measurements of yaw were made using a single hot wire. This was rotated to two positions, about 90° apart, which gave the same voltage reading. The direction of flow was taken as the mean of these two angular positions. The uncertainty in the measurements using this method was probably $\pm 1°$ in yaw. Yaw angles measured in this way were then used in conjunction with the readings of total pressure already obtained by the three-hole probe to obtain velocity profiles in tangential and radial directions. The general arrangement of the apparatus is shown in figure 2.

To overcome the difficulty in fixing accurately the direction corresponding to the zero reading of the yawmeters, they were calibrated *in situ*. The air stream was provided by blowing through a 2 in. diameter brass pipe, about 2 ft. long, which was aligned carefully at right angles to the radial travel of the probes provided by the traversing mechanism. The inlet end of the pipe was fitted with a reducer leading from a 4 in. diameter pipe in which honeycombs were fitted.

Air was supplied by a small centrifugal fan whose flow rate could be controlled. The direction of the stream in the brass pipe was determined consistent to $\pm 0{\cdot}5°$ by the hot-wire technique for a wide range of air speeds. It was also repeatable for a different radial position of the probe. The alignment of the pipe was true to $\pm 0{\cdot}1°$.

A check on the calibrations and the behaviour of the probes was made by traversing the boundary layer in the laminar region. This was particularly useful in giving a reasonable estimate of the position of the effective centre of the flattened pitot. From the comparisons between the measurements and laminar

theory shown in figures 3 and 4, it may be concluded that the experimental accuracy was satisfactory.

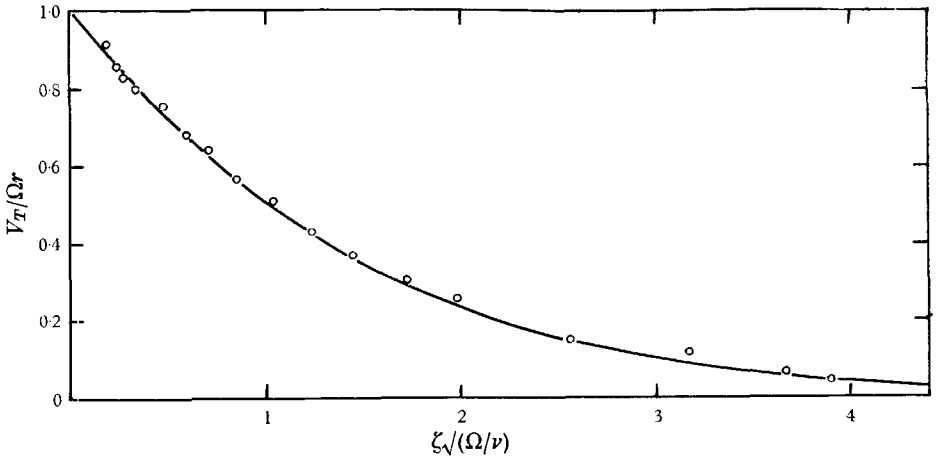

FIGURE 3. Velocity magnitude v_T in the laminar boundary layer. ——, theory; ○, experiment at 515 rev/min, radius 7·5 in., $R_r = 1{\cdot}29 \times 10^5$.

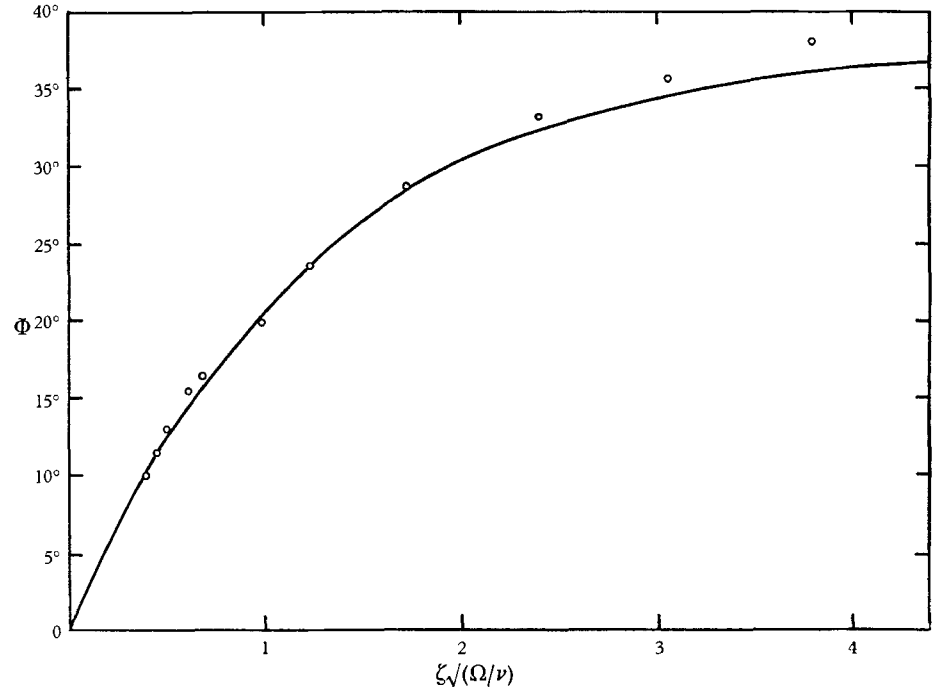

FIGURE 4. Flow direction in the laminar boundary layer. ——, theory; ○, experiment at 515 rev/min, radius 7·5 in., $R_r = 1{\cdot}29 \times 10^5$.

6. Experimental measurements

Traverses of the boundary layer were made at three rotational speeds (515, 1000 and 1550 rev/min) and at three radii on the disk for each speed. The range of R_r ($\equiv \Omega r^2/\nu$) covered was from 3×10^5 to 2×10^6. A check was made to ensure

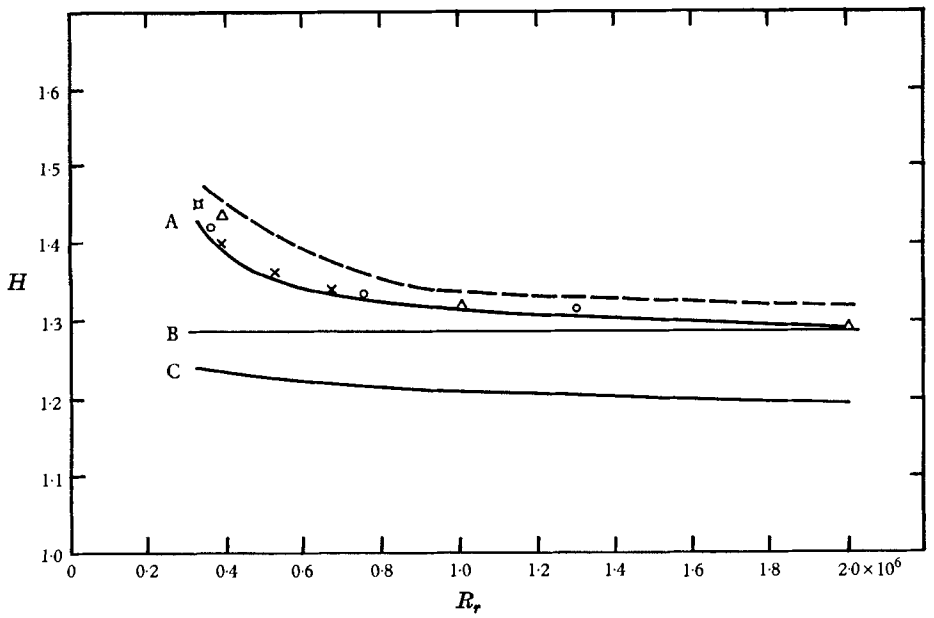

FIGURE 5. Development of the shape factor for circumferential velocity profiles. A, present calculation using the entrainment method; B, von Kármán (1921) and Banks & Gadd (1962); C, Goldstein (1935); ———, calculation with isotropic eddy viscosity; ⊡, experiments of Gregory *et al.* (1955). Present experiments: ×, 515 rev/min; ○, 1000 rev/min; △, 1550 rev/min.

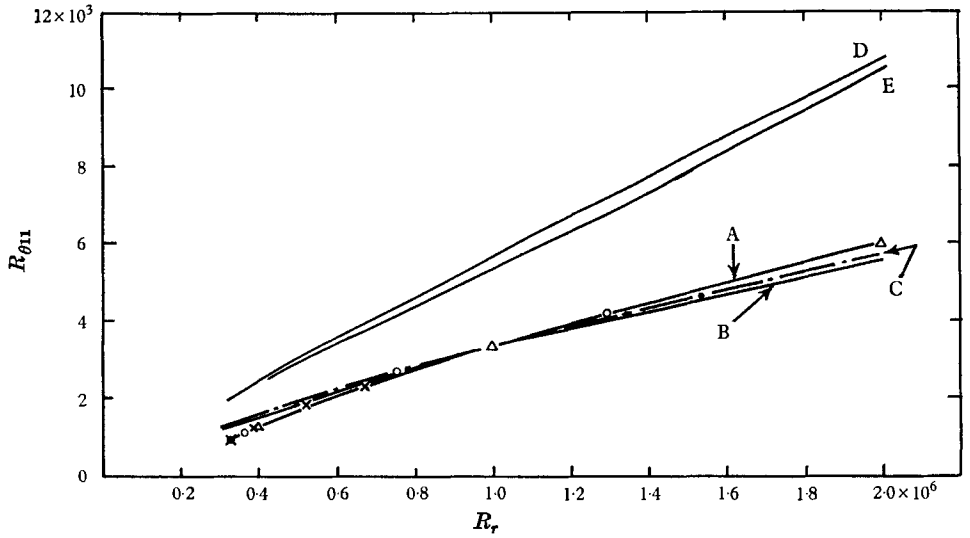

FIGURE 6. Development of the circumferential momentum thickness with Reynolds number. A, present calculation; B, von Kármán (1921); C, Banks & Gadd (1962); D, Goldstein (1935); E, Dorfman (1963); ⊠, experiments of Gregory *et al.* (1955). Present experiments: ×, 515 rev/min; ○, 1000 rev/min; △, 1550 rev/min.

that the positions where the readings were taken were within the turbulent régime by listening for the turbulent roar through a stethoscope connected to a hand-held Pitot. The extent of the turbulent region was also confirmed visually by the use of paraffin evaporating from a coating of china-clay.

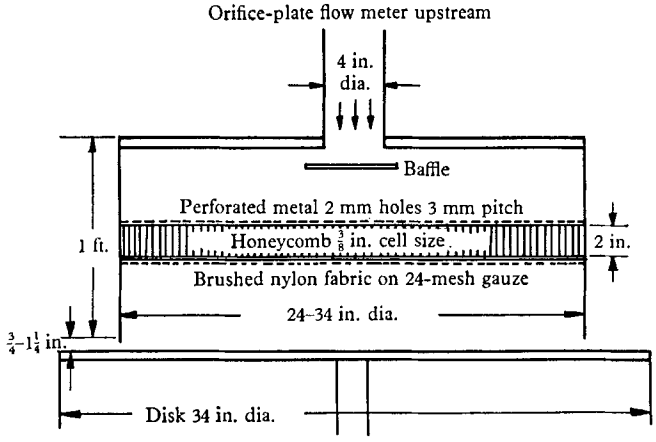

FIGURE 7. Arrangement for the direct measurement of entrainment.

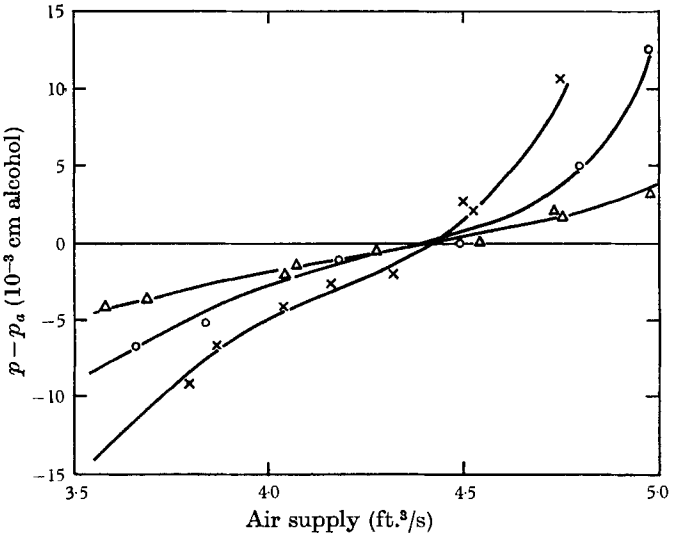

FIGURE 8. Pressure difference as a function of flow rate for various clearances: ×, ⅞ in.; ○, 1 in.; △, 1¼ in. Drum radius 17 in., disk speed 1200 rev/min, $R_r = 1{\cdot}543 \times 10^6$.

The circumferential and cross-flow components of velocity were deduced by taking the cosine and sine functions of the yaw angle with the total velocity. As a result of using a sine function of small angles, the form of cross-flow profile was very sensitive to the accuracy of the angles obtained. This was not the case for the circumferential component.

Experimental mean velocity profiles for the rotational speed of 1550 rev/min are shown in figures 11 and 12. There is comparatively little experimental

scatter, except at the outer edge of the boundary layer. The cross-flow profiles show a slight variation in shape from the 'rounded peak' profiles at higher R_r to the 'sharp-peak' ones near to transition. All the cross-flow profiles have a point

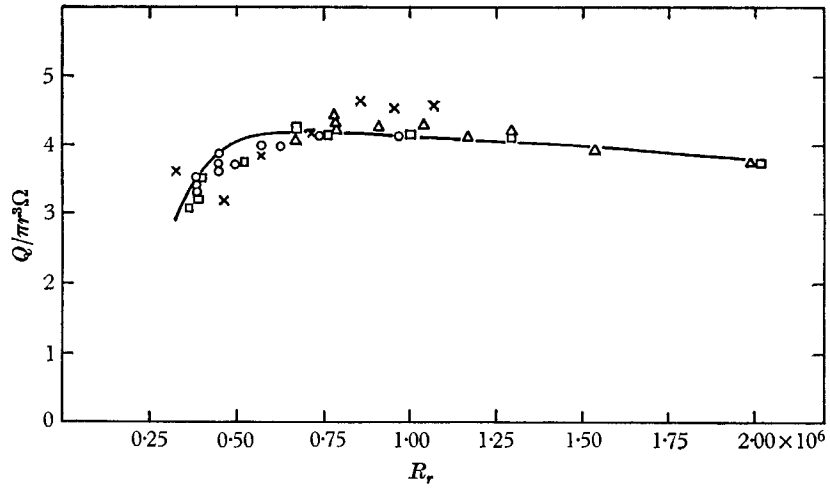

FIGURE 9. Dimensionless entrainment as a function of Reynolds number. ——, curve used in the calculations. Experimental results: ○, 12 in. radius drum; △, 17 in. radius drum; □, from the cross-flow profiles; ×, Case (1966).

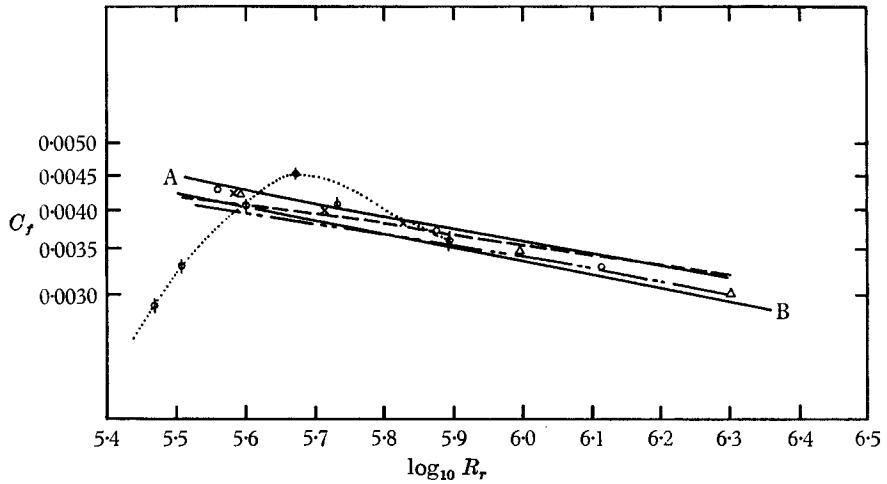

FIGURE 10. Development of the circumferential skin-friction component. —— A, present calculation using the entrainment method; —— B, von Kármán (1921); ———, Goldstein (1935); ----, calculation, with isotropic eddy viscosity; .. Φ .., Theodorsen & Regier (1944). Results taken from Clauser plots of the present measurements: ×, 515 rev/min; ○, 1000 rev/min; Δ, 1550 rev/min.

of inflexion and agree fairly well with the form of cross-flow suggested by Mager (1952). It is interesting to note that the circumferential velocity profiles correspond very closely to Thompson's velocity profiles for two-dimensional flow.

The shape factor H, and $R_{\theta 11}$ based on the streamwise component of the velocity, were evaluated and their variations with R_r are shown in figures 5 and 6.

Entrainment measurements

Direct measurements of the entrainment of external fluid into the boundary layer were made employing essentially the same technique as that of Case (1966). The details are given in figure 7. The principle consists in blowing air into the

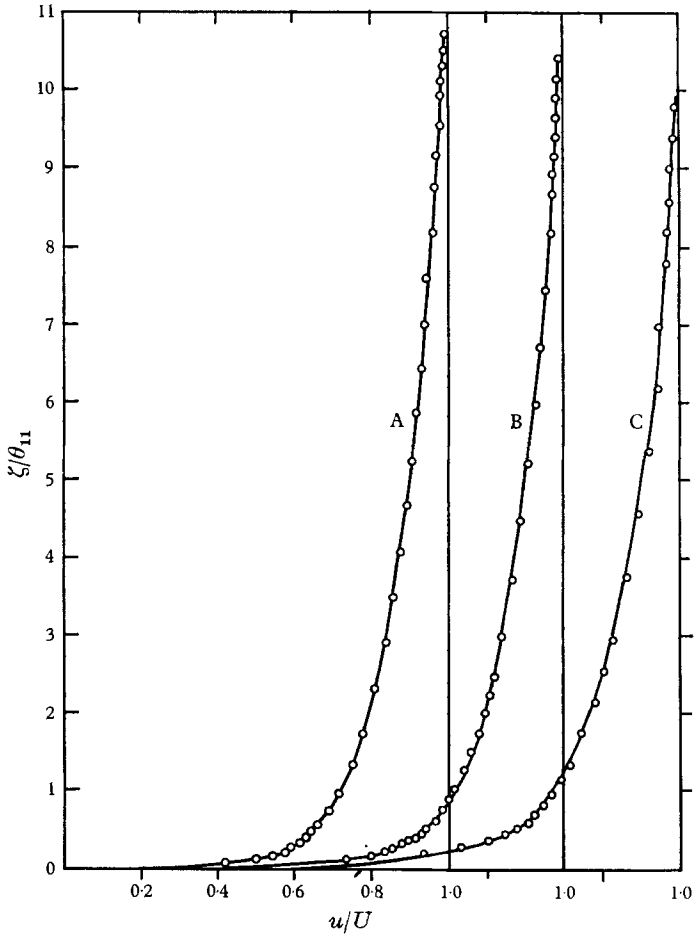

FIGURE 11. Circumferential velocity profiles at 1550 rev/min; ——, theory; ○, experiment. Curve A, r = 17 in., H = 1·29, $R_{\theta 11}$ = 6000; curve B, r = 12 in., H = 1·32, $R_{\theta 11}$ = 3350; curve C, r = 7·5 in., H = 1·43, $R_{\theta 11}$ = 1278.

drum, which is just clear of the boundary layer, at such a rate as to balance the intake of air into the boundary layer. When this condition is satisfied, the static pressure in the chamber is atmospheric. Two different sizes of drum (12 in. radius and 17 in. radius) were used, the flow being smoothed by honeycombs and screens as well as a baffle at entry.

The test method consisted of using either of the two drums and rotating the disk at a series of speeds, for each of which the quantity of air blown into the chamber was varied and the static pressure in the drum recorded. This procedure was repeated for different clearances between the drum and the boundary layer. A typical result is shown in figure 8, and it will be seen that the flow rate for

atmospheric pressure in the drum is independent of the gap between the drum and the surface of the disk, provided the lower edge of the drum is clear of the boundary layer.

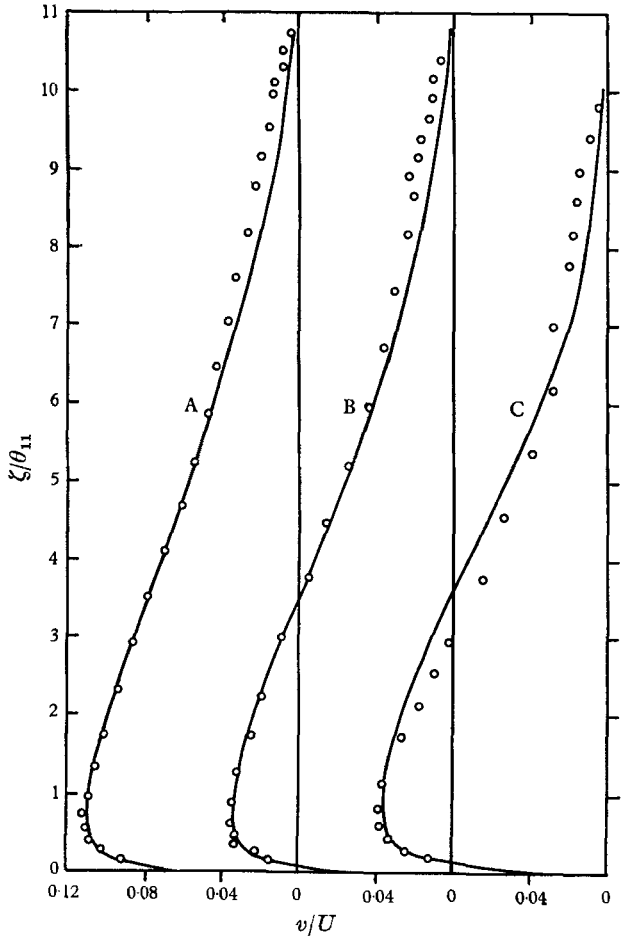

FIGURE 12. Cross-flow velocity profiles at 1550 rev/min. ——, theory; ○, experiment. Curve A, $r = 17$ in., $R_r = 2 \times 10^6$; curve B, $r = 12$ in., $R_r = 9{\cdot}95 \times 10^5$; curve C, $r = 7{\cdot}5$ in., $R_r = 3{\cdot}38 \times 10^5$.

The entrainment was also deduced from the yawmeter and the total pressure traverses through the boundary layer on the disk in free air, the integrated cross-flow component of the velocity distribution through the layer evidently representing the entrainment up to the radius at which the traverses were performed.

The results of the measurements, both direct and indirect, are shown in figure 9, and it is seen that they show relatively little scatter and are in broad agreement with those of Case (1966) though much more consistent. It may be noted that they are also in close agreement with the theoretical prediction based on the $(C_E, H_{\delta-\delta_1^*})$ entrainment curve used in the calculations (figure 1) and Mager's cross-flow model. This may also be deduced from the agreement of the cross-flow velocity profiles shown in figure 12.

Circumferential component of wall shear stress

In order to check whether the streamwise component of a three-dimensional turbulent boundary layer obeys the logarithmic law of the wall, the streamwise profile (figure 11) was plotted in the form first suggested by Clauser (1954). Typical distributions are shown in figure 13. They conform to the normal two-dimensional shape with three distinct regions which are the sub-layer, the wall region and the wake region. For each of the velocity profiles, as there is a fairly

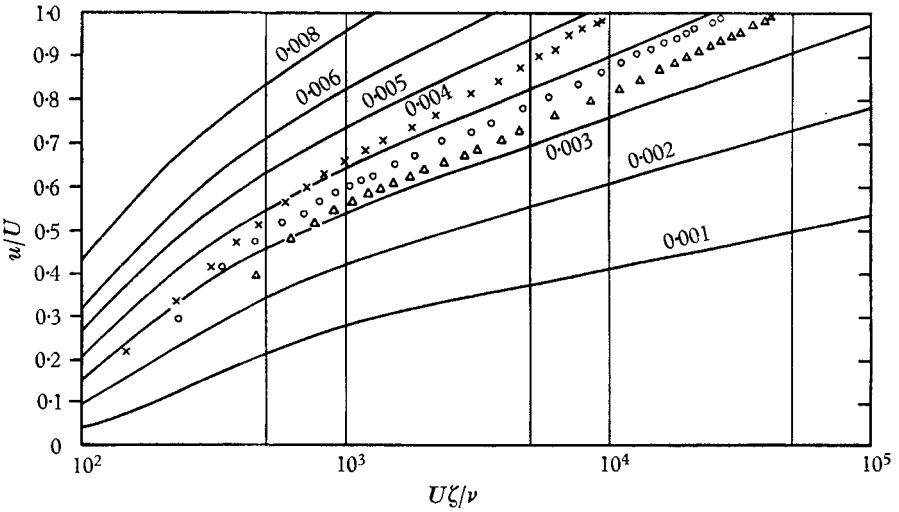

FIGURE 13. Clauser plot of circumferential velocity profiles at 1000 rev/min. ×, r = 9 in.; ○, r = 13 in.; Δ, r = 17 in.

extensive linear portion oriented at more or less the required slope, it is possible to deduce values of C_{f1}, assuming that the same law of the wall holds for the streamwise velocity component as for a two-dimensional turbulent boundary layer. The experimental values of C_{f1} obtained in this way are shown in figure 10, and it is seen that the values are realistic.

Surface streamlines

As it was difficult to deduce accurately the direction of the surface streamlines from the velocity measurements, a visual method was attempted using the azo-benzene sublimation technique. Artificial roughnesses of height varying from 0·003 in. to 0·02 in. were glued on the surface of the disk at a radius of 13·5 in. The disk was rotated at 1000 rev/min for about one hour after the azo-benzene was sprayed on. When the disk was stopped, faint lines of about 0·4 in. long could be seen on the surface extending from the roughnesses in the direction of flow relative to the disk. For a height of roughness element less than about 0·005 in., the trace was too faint for its direction to be accurately measured. All the other roughnesses showed a flow direction of between 10·5° and 12° to the circumferential direction.

However, from the estimated value of U_τ, it appears that, in fact, the rough-

nesses that gave useful results all protruded through the laminar sub-layer and the measured angles are therefore unlikely to represent the true limiting values at the surface. A height of 0·005 in. is just outside the sub-layer, if this is based on a value of $U_\tau \zeta/\nu = 8$.

7. Calculation using eddy viscosity

An exploratory attempt was made to calculate the turbulent boundary layer by using the concept of locally isotropic eddy viscosity in place of the empirical Mager cross-flow profile. Because of the complexity of the calculation procedure and because the initial interest was in the cross-flow velocity profile, no direct calculations of boundary-layer development were made. Instead, the radial developments of circumferential momentum thickness already calculated were used, along with present hypothesis, to calculate cross-flow velocity profiles and the corresponding values of H for the circumferential profiles, which were again represented by Thompson's profile family. Further details of the calculation procedure can be obtained from Cham (1968).

The results of the calculations of cross-flow profiles are shown in figures 14 and 17. All show a slight overestimation of the cross-flow velocities, with the greatest discrepancy at the lower Reynolds numbers. Nevertheless, the general form of the calculated cross-flow profiles is plausible, and corresponds in essential features with both Mager's cross-flow model and the experimental profiles. On the whole, however, the results appear to be in no way superior to those obtained by the simpler procedure.

8. Comparison of theories with experiment

Although there is no *a priori* analytical evidence that the turbulent boundary layer on a rotating disk can be treated as a function of the single variable R_r, the experimental results positively indicated this to be the case. This, of course, is only possible if the Reynolds number at transition does not vary with rotational speed.

Referring to figures 5 and 6, it is clear that the calculations based on entrainment predict the H and $R_{\theta 11}$ developments of the turbulent boundary layer with considerable accuracy. Especially significant is the H value near transition compared to those at higher values of R_r. The calculation based on isotropic eddy viscosity, as outlined in § 7, gives a higher H throughout but nevertheless shows the same trend. Von Kármán, and Banks & Gadd provide a reasonably good prediction of the growth of streamwise momentum thickness but their theories give a poor description of the velocity profile shape factor for the lower Reynolds numbers. Evidently any theory that is based essentially on turbulent boundary-layer properties appropriate to high Reynolds numbers would not expect to give good agreement over the whole range considered here.

The skin friction values predicted by all the theories are in reasonable agreement as shown in figure 10. It is impossible to rate the theories by this test since there are no measurements of the required accuracy. As shown in the plots given

by Goldstein (1935) and Dorfman (1963), the experimental scatter is as great as the differences between the theories.

As pointed out earlier, the measured streamwise velocity profiles are represented with considerable accuracy by Thompson's two-dimensional profile family. The experimental cross-flow profiles, as shown in figure 12, agree reason-

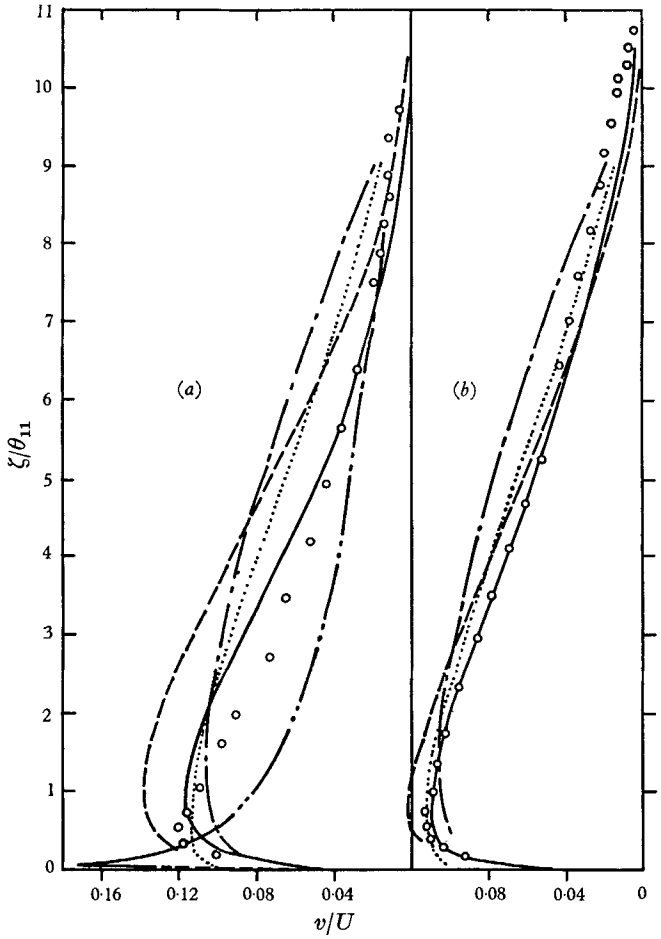

FIGURE 14. Comparison of cross-flow profiles. (*a*) $R_r = 3{\cdot}6 \times 10^5$; (*b*) $R_r = 2 \times 10^6$. ○, experiment; ——, present calculation using the entrainment method; — — —, calculation with isotropic eddy viscosity; —·—, von Kármán (1921); —··—, Goldstein (1935); ....., Banks & Gadd (1962).

ably closely with Mager's cross-flow model, showing that this is also applicable with rotating surfaces. The cross-flow profiles given by other theories are also shown in figure 14, one at the highest and one at the lowest Reynolds number measured. The discrepancies are seen to be greater at the lower Reynolds number. Undoubtedly, the theory based on entrainment and Mager's quadratic expression for the cross-flow gives the best overall agreement. Polar plots of the velocities at the two extremes of Reynolds number are shown in figure 15 and correspond reasonably closely to the triangular model suggested by Johnston (1960).

Referring to figure 16, it is seen that there are great differences between the different theories in predicting the angle of the surface streamline. Present results and the calculations by Banks & Gadd (1962) give values within the range indicated by the flow visualization experiment. However, as pointed out earlier, the

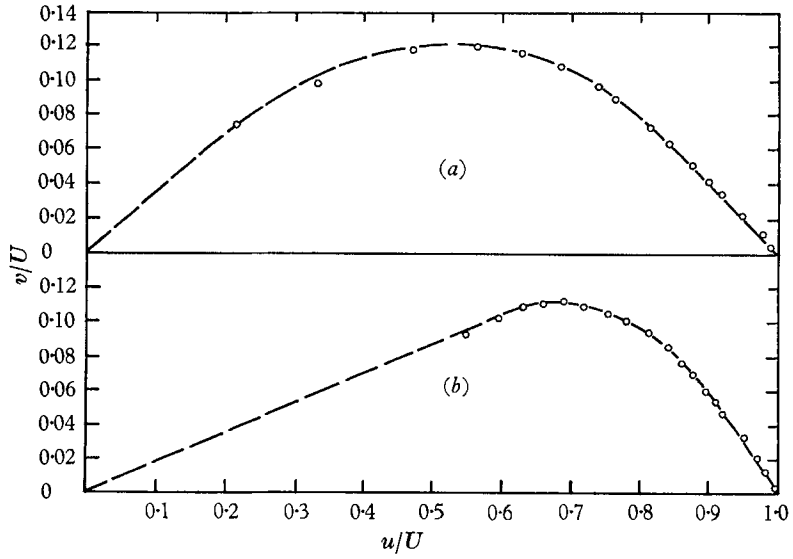

FIGURE 15. Polar plots of measured velocities. (*a*) $R_r = 3{\cdot}61 \times 10^5$; (*b*) $R_r = 2 \times 10^6$.

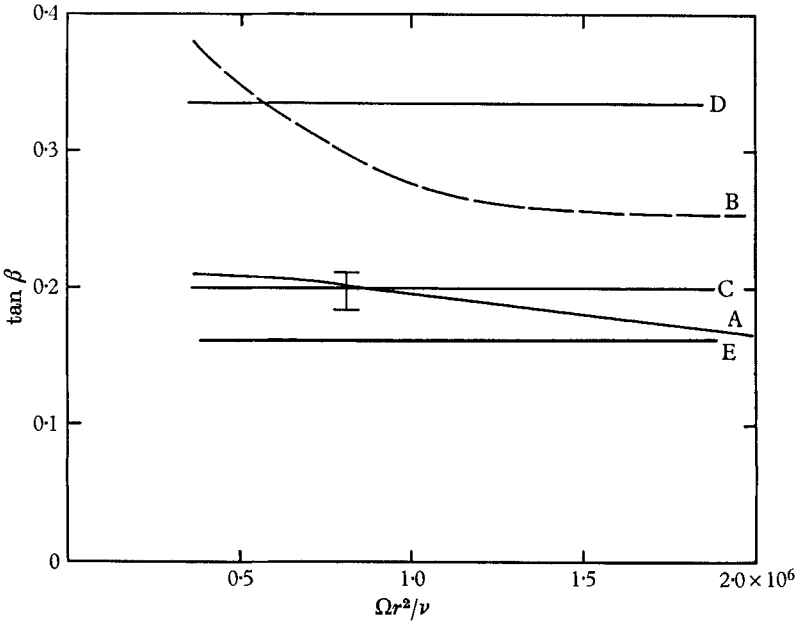

FIGURE 16. Angles of surface streamlines. I, experiment; A, present calculation using the entrainment method; B, calculation with isotropic eddy viscosity; C, Banks & Gadd (1962); D, Goldstein (1935); E, von Kármán (1921).

experimental results do not give the true values at the surface but some value at the edge of the sub-layer. As shown by Cham (1968), it seems likely that there should be an appreciable difference between the two values. No conclusive comparisons can therefore be made between the different theories.

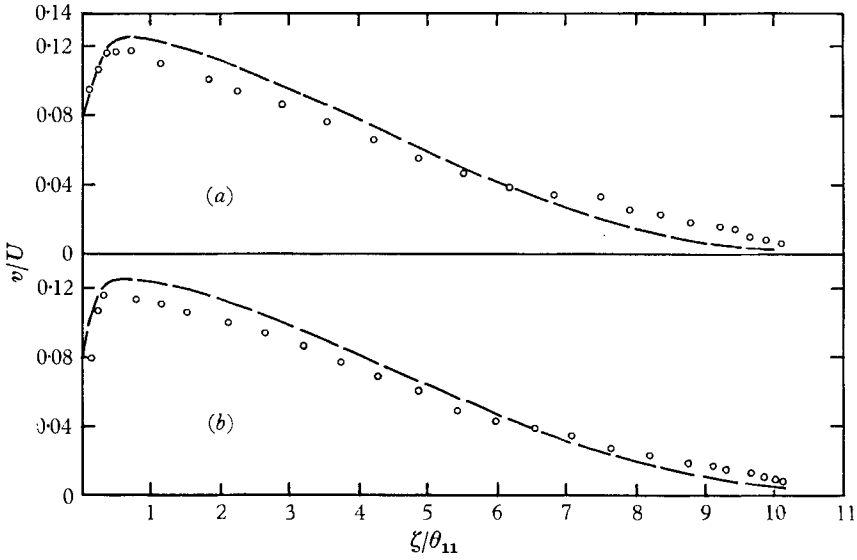

FIGURE 17. Cross-flow velocity profiles at intermediate Reynolds numbers. (*a*) $R_r = 7{\cdot}52 \times 10^5$; (*b*) $R_r = 1{\cdot}29 \times 10^6$. ——, calculation using isotropic eddy viscosity; ○, experiment.

It is seen that the entrainment method, which gives fairly good predictions for two-dimensional turbulent boundary layers, can be extended to three-dimensional flow, but it is also apparent that the entrainment rate is affected by the three dimensionality of the problem. Although C_E still varies in the same way with $H_{\delta-\delta^*}$ as in two-dimensional flow, there is a reduction in actual magnitude of about 30 %. Provided this reduction in entrainment is incorporated, the present calculation gives a good overall prediction of the development of the turbulent boundary layer on a rotating disk.

9. Conclusions

The use of an entrainment equation together with the circumferential and radial momentum integral equations enable the development of the turbulent boundary layer over a disk rotating in free air to be simply calculated. The technique of solution is essentially a simultaneous solution of the equations for each radius.

Based on the assumption that the entrainment depends only on the streamwise component of the velocity profile, a decrease of about 30 % in the entrainment rate proposed by Head (1958) for two-dimensional boundary layers is necessary in order to obtain the best overall agreement between theory and experiment. This reduction is confirmed experimentally by direct measurements of entrain-

ment. When this allowance is made, the shape factor H, the Reynolds number $R_{\theta 11}$ and the predictions of cross-flow are in virtually perfect agreement with the experimental values. The circumferential- and radial-flow velocity profiles are well represented by Thompson's two-parameter family and Mager's cross-flow expression respectively. The present calculations are in significantly better agreement with experiment than any previous theories for the rotating disk.

From the experimental and theoretical results, it is evident that the turbulent boundary layer on a rotating disk can be treated as a function of one variable R_r, the Reynolds number based on the radius.

REFERENCES

BANKS, W. H. & GADD, G. E. 1962 A preliminary report on boundary layers on screw propellers and simpler rotating bodies. *Nat. Phys. Lab. Ship Div. Rep.* no. 27.

CASE, P. 1966 Measurements of entrainment by a free rotating disc. *J. Roy. Aero Soc.* **71**, 124.

CHAM, T-S. 1968 Turbulent boundary layers in rotating flows. Ph.D. thesis, Cambridge University.

CLAUSER, F. H. 1954 Turbulent boundary layers in adverse pressure gradients. *J. Aero. Sci.* **21**, 91–108.

COCHRAN, W. G. 1934 The flow due to a rotating disk. *Proc. Camb. Phil. Soc.* **30**, 365–75.

CUMPSTY, N. A. & HEAD, M. R. 1967 The calculation of three-dimensional turbulent boundary layers, pts 1 and 2. *Aero. Quart.* **18**, 55–84, 150–164.

DORFMAN, L. A. 1963 *Hydrodynamic Resistance and the Heat Loss of Rotating Solids.* Oliver and Boyd.

GOLDSTEIN, S. 1935 On the resistance to the rotation of a disk immersed in a fluid. *Proc. Camb. Phil. Soc.* **31**, 232.

GREGORY, N., STUART, J. T. & WALKER, W. S. 1955 On the stability of three-dimensional boundary layers with application to the flow due to a rotating disk. *Phil. Trans.* A **248**, 155–99.

HEAD, M. R. 1958 Entrainment in the turbulent boundary layer. *Aero. Res. Coun. R & M* no. 3152.

JOHNSTON, J. P. 1960 On the three-dimensional turbulent boundary layer generated by secondary flow. *ASME, J. Basic Engng.* **82**, 233–248.

KÁRMÁN, TH. VON 1921 Über laminare und turbulente Reibung. *ZAMM*, **1**, 233.

KEMPF, G. VON 1922 Über Reibungswiderstand rotierender Scheiben. Vortrage aus dem Gebiete der Hydro und Aerodynamik, Innsbruck.

MAGER, A. 1952 Generalisation of boundary layer momentum-integral equations to three-dimensional flows including those of rotating system. *NACA Rep.* no. 1067.

ROSENHEAD, L. 1963 *Laminar Boundary Layers.* Oxford University Press.

SCHMIDT, W. 1921 Ein einfaches Messverfahren für Drehmomente. *ZVDI*, **65**, 441.

STAIN, W. C. 1961 The three-dimensional turbulent boundary layer on a rotating disk. *Aerophysics Department, Mississippi State University, Res. Rep.* no. 35.

THEODORSEN, T. & REGIER, A. 1944 Experiments on drag of revolving disks, cylinders and streamline rods at high speeds. *NACA Rep.* no. 793.

THOMPSON, B. G. J. 1965 A new two-parameter family of mean velocity profiles for incompressible turbulent boundary layers on smooth walls. *Aero. Res. Coun. R & M* no. 3463.